Advances in Water Resources 96 (2016) 180–189

Contents lists available at ScienceDirect

Advances in Water Resources

journal homepage: www.elsevier.com/locate/advwatres

Upscaling of solute transport in disordered porous media by wavelet transformations

Mahsa Moslehi[a], Felipe P.J. de Barros[a,*], Fatemeh Ebrahimi[b], Muhammad Sahimi[c]

[a] Sonny Astani Department of Civil and Environmental Engineering, University of Southern California, Los Angeles, California 90089 2531, USA
[b] Department of Physics, Faculty of Sciences, University of Birjand, Birjand 97178 51367, Iran
[c] Mork Family Department of Chemical Engineering and Materials Science, University of Southern California, Los Angeles, California 90089 1211, USA

ARTICLE INFO

Article history:
Received 29 March 2016
Revised 21 July 2016
Accepted 21 July 2016
Available online 22 July 2016

Keywords:
Flow and transport
Heterogeneous porous media
Upscaling wavelet transform
Computational efficiency

ABSTRACT

Modeling flow and solute transport in large-scale (e.g.) on the order of 10^3 m heterogeneous porous media involves substantial computational burden. A common approach to alleviate the problem is to utilize an upscaling method that generates models that require less intensive computations. The method must also preserve the important properties of the spatial distribution of the hydraulic conductivity (K) field. We use an upscaling method based on the wavelet transformations (WTs) that coarsens the computational grid based on the spatial distribution of K. The technique is applied to a porous formation with broadly distributed and correlated K values, and the governing equation for solute transport in the formation is solved numerically. The WT upscaling preserves the resolution of the initial highly-resolved computational grid in the high K zones, as well as that of the zones with sharp contrasts between the neighboring K, whereas the low-K zones are averaged out. To demonstrate the accuracy of the method, we simulate fluid flow and nonreactive solute transport in both the high-resolution and upscaled grids, and compare the concentration profiles and the breakthrough times. The results indicate that the WT upscaling of a K field generates non-uniform upscaled grids with a number of grid blocks that on average is about two percent of the number of the blocks in the original high-resolution computational grids, while the concentration profiles, the breakthrough times and the second moment of the concentration distribution, computed for both models, are virtually identical. A systematic parametric study is also carried out in order to investigate the sensitivity of the method to the broadness of the K field, the nature of the correlations in the field (positive versus negative), and the size of the computational grid. As the broadness of the K field and the size of the computational domain increase, better agreement between the results for the high-resolution and upscaled models is obtained.

1. Introduction

It is of fundamental and practical importance to incorporate the spatial heterogeneity of porous geological formations in the models of flow and transport in such media (Dagan et al., 1989; Rubin, 2003; Sahimi, 2011). At the field scale (e.g. orders of $10^2 - 10^3$ m), subsurface properties, such as the permeability, vary many orders of magnitude across multiple length scales (e.g. from 1 m to 10^3 m or larger) (Dagan et al., 1989; Rubin, 2003; Sahimi, 2011). It is well recognized that the spatial fluctuations of the permeability field, i.e. many orders of magnitude difference between permeability values, have a significant role in the spreading rates of solute plumes, as well as estimates of their early or late arrival times. Thus, neglecting the effect of subsurface heterogeneity, and in particular the spatial distribution of the permeability, in numerical simulation leads to erroneous prediction of solute transport, which will have severe consequences for health risk assessment (de Barros and Rubin, 2008; Maxwell et al., 1999), the likelihood of extreme events (de Barros and Fiori, 2014; Dentz and Tartakovsky, 2010; Henri et al., 2015), and for reactive mixing (Dentz et al., 2011; Luo et al., 2008).

In general, to obtain accurate predictions for solute mixing at the field scale and calculate the properties that characterize the process, such as the distribution of travel times and the dispersion coefficients, numerical simulation of flow and transport in large-scale porous media requires a computational grid with high enough resolution to represent the variability of the hydrogeological properties (Ababou et al., 1989; de Dreuzy et al., 2007). Simulation with such high-resolution computational grids entails solving

* Corresponding author.
E-mail addresses: moslehi@usc.edu (M. Moslehi), fbarros@usc.edu (F.P.J. de Barros), f_ebrahimi@birjand.ac.ir (F. Ebrahimi), moe@usc.edu (M. Sahimi).

http://dx.doi.org/10.1016/j.advwatres.2016.07.013
0309-1708/

several million discretized equations over thousands of time steps, leading to a very high computational burden. The resolution of the grid depends, of course, on the available data that are used to construct the grid blocks. But, for the same of argument we consider blocks whose linear size is 1 m. Thus, numerical simulation of solute transport at the field scale might become prohibitively expensive, particularly when such highly-resolved models are subject to uncertainty and must be cast within a Monte Carlo sampling (Rubin, 2003; Sahimi, 2011). As a result, a key aspect of the simulation is how to distribute the limited computational resources in an efficient manner in order to reduce the simulation cost (Leube et al., 2013; 2012; Moslehi et al., 2015). To alleviate the computational burden, upscaling methods are used.

Upscaling flow and transport in heterogeneous porous formations has been studied intensively for several decades. One may divide the existing methods into those that are based on volume (Wang and Kitanidis, 1999; Whitaker, 1999; Wood et al., 2003; Wood and Valdés-Parada, 2013), ensemble (Koch and Brady, 1985; Rubinstein and Torquato, 1989), or stochastic averaging (Attinger, 2003; Dagan, 1984; Gelhar and Axness, 1983; Neuman et al., 1987; Rubin et al., 1999). In the context of stochastic averaging, many analytical methods have been developed to evaluate the effective transport properties in a coarse-scale heterogeneous model, including analytical perturbation (de Barros and Dentz, 2016; de Barros and Rubin, 2011; Gelhar and Axness, 1983; Gutjahr et al., 1978) and self-consistent (Dagan et al., 1989; Fiori et al., 2011; Rubin and Gómez-Hernández, 1990) methods. Alternatively, numerical simulations (Ababou, 1988; Desbarats, 1987; Warren et al., 1961) and the renormalization group transformations (King, 1989; King et al., 1993; Mukhopadhyay and Sahimi, 2000) have been employed to compute the effective conductivity of field-scale porous media. Such works were reviewed by Renard and De Marsily (1997), Wen and Gómez-Hernández (1996), and Sahimi (2011).

In general, most of the coarsening process is carried out by homogenizing the aquifer's model through, for example, its hydraulic conductivity or the permeability attributed to the blocks of a highly-resolved computational grid such that the upscaled permeability or conductivity field has identical symmetries as those of the fine-scale field, as defined earlier (Desbarats, 1992; Durlofsky, 1991; Kitanidis, 1990). The size of the upscaled grid blocks is determined by considering the available computational resources. A drawback associated with the homogenization techniques is that they coarsen the subsurface domain uniformly, which often leads to large errors in the predictions for the flow and transport properties, especially in the presence of fractured regions or sink and source. This is because many homogeneization methods average out the effects of extreme events, such as fast flow paths or large flow barriers. To address this issue, Durlofsky et al. (1997) proposed to first scale up the permeability field by a homogenization technique and then identify the high-velocity regions by solving for single-phase flow in the homogenized grid. Such regions are then discretized to the fine scale in order to capture the small-scale variability that the field contains. Although the issue of uniform blocks is addressed, the single-phase flow should still be computed prior to the upscaling process.

An alternative method for upscaling is based on the wavelet transforms (WTs) (Ebrahimi and Sahimi, 2002; 2004; 2006; Heidarinasab et al., 2004; Mehrabi and Sahimi, 1997; Rasaei and Sahimi, 2008; 2009; Sahimi, 2003), which have been used to upscale heterogeneous porous media by coarsening the permeability or hydraulic conductivity field. The method upscales the high-resolution geological model of a porous formation non-uniformly, which leads to preserving the important information on the spatial distribution of the permeability field at all the relevant length scales, but coarsens those parts of the computational grid that contribute little to the flow field. Thus, the number of grid blocks in the computational grid and, hence, the number of flow and transport equations to be solved are reduced drastically without sacrificing any crucial information about the conductivity or permeability field. Use of the WTs in various applications has been the subject of intensive research over the past 25 years (Chui, 1992; Heidarinasab et al., 2004; Holschneider, 1995; Meyer, 1992; Nievergelt and Nievergelt, 1999; Sahimi, 2003), including the simulation of flow and transport in large-scale porous media, such as oil reservoir (Kikani et al., 1998; Lu et al., 2000; Moridis et al., 1996; Rasaei and Sahimi, 2008, 2009; Sahimi, 2003; Sahimi and Hashemi, 2001).

The focus of this study is to extend the upscaling method by the WTs, introduced originally by Mehrabi and Sahimi (1997) and Ebrahimi and Sahimi (2002), to upscaling of solute transport in disordered porous media. Their work focused on upscaling a permeability or conductivity field. In contrast, our primary goal is to investigate the effect of multiple features, i.e. structural and geometrical parameters, in the conductivity field on the overall transport behavior, such as the arrival time, peak concentration and spatial moments, and to demonstrate how geostatistical parameters characterizing the heterogeneous fields influence the performance of the upscaling using wavelet transformation. Furthermore, we used the upscaled field to reconstruct the second central spatial moment of the plume that represents global features of the transport process. The spatial moment analysis has not be been analyzed in the previous works related to WTs. We show that upscaling by the WTs efficiently coarsens the computational grid for simulating solute transport in subsurface domains, and reduces substantially the number of grid blocks. To demonstrate the accuracy of the upscaling procedure via the WTs, flow and transport are simulated in both the fine-resolution and the upscaled computational grids, and the results are compared.

The rest of this paper is structured as follows. In Section 2 we formulate the class of problem under investigation. Section 3 describes the details pertaining to the WTs and the methodology used for upscaling of the hydraulic conductivity or permeability field. We then present the details of the numerical simulations in Section 4. The results are presented and discussed in Section 5, where we test systematically the performance of the WT upscaling for a variety of disordered porous formations. The last section summarizes the paper.

2. Problem statement

We consider a fully-saturated steady-state flow of an incompressible and Newtonian fluid through a heterogeneous geological formation. The hydraulic conductivity $K(\mathbf{x})$ is spatially distributed, where $\mathbf{x}$ represents the Cartesian coordinate system. We assume that the flow is slow enough that the fluid velocity $\mathbf{v}(\mathbf{x})$ follows the Darcy's law

$$\mathbf{v}(\mathbf{x}) = \frac{K(\mathbf{x})}{\mathcal{P}} \nabla \varphi(\mathbf{x}) \,, \tag{1}$$

where $\varphi(\mathbf{x})$ is the hydraulic head, and $\mathcal{P}$ is the porosity of the medium, assumed to be uniform. As usual, the hydraulic head is computed by solving the flow equation

$$\nabla \cdot [K(\mathbf{x}) \nabla \varphi(\mathbf{x})] = 0 \,. \tag{2}$$

A constant hydraulic gradient in the mean sense is imposed on the system such that, on average, the flow is uniform along the longitudinal direction. An inert solute is released and advected and dispersed by the fluctuating velocity field and diffusion. The spatiotemporal evolution of the concentration field is governed by the advection-dispersion equation,

$$\frac{\partial C(\mathbf{x}, t)}{\partial t} + \mathbf{v}(\mathbf{x}) \cdot \nabla C(\mathbf{x}, t) = \nabla \cdot [\mathbf{D}_o(\mathbf{x}) \nabla C(\mathbf{x}, t)] \,, \tag{3}$$

where $C(\mathbf{x}, t)$ is the solute concentration at point $\mathbf{x}$ at time t, and $\mathbf{D}_o(\mathbf{x})$ is the local dispersion tensor. Alternatively, transport can be formulated in terms of the Langevin equation (Risken, 1984),

$$\frac{d\mathbf{x}(t|\mathbf{a})}{dt} = \mathbf{v}[\mathbf{x}(t|\mathbf{a})] + \sqrt{2\mathbf{D}_o}\eta(t), \tag{4}$$

where $\mathbf{x}(t)$ is the position of the particles, $\mathbf{a}$ is the initial location of the solute particle (i.e. $\mathbf{x}(0|\mathbf{a}) = \mathbf{a}$) and $\eta(t)$ is the Gaussian white noise characterized by zero mean and covariance $\langle \eta_i(t)\eta_j(t')\rangle = \delta_{ij}\delta(t-t')$ where δ_{ij} is the Kronecker delta, $\delta(t)$ is the Dirac delta distribution and $\langle \cdot \rangle$ indicates the average over all noise realizations (i.e. $\eta(t)$). In order to obtain an accurate solution for $C(\mathbf{x}, t)$, a highly-resolved (i.e. fine-scale) representation of $K(\mathbf{x})$ is generated, which is then upscaled while maintaining the key features of its variations that produce the concentration field.

3. Methodology

Let us first briefly describe the WTs, and then explain the upscaling method.

3.1. Wavelet transformations

For an excellent introduction to the WTs and their properties see Nievergelt (1999). We define the WT of the spatially-varying permeability or hydraulic conductivity $K(\mathbf{x})$, also referred to as the *wavelet detail coefficient*, by

$$\mathcal{D}(a, \mathbf{b}) = \int_{-\infty}^{\infty} K(\mathbf{x})\psi_{ab}(\mathbf{x})d\mathbf{x} = \frac{1}{\sqrt{a}}\int_{-\infty}^{\infty} K(\mathbf{x})\psi[(\mathbf{x}-\mathbf{b})/a]d\mathbf{x}\,, \tag{5}$$

where $\psi(\mathbf{x})$ is usually called the *mother wavelet*. The choice of $\psi(\mathbf{x})$ depends on the intended application and, in fact, the possibility of developing separate wavelets for each application is a great advantage of the WT. Eq. (5) makes it clear that $a > 0$ is a rescaling parameter, whereas $\mathbf{b}$ represents translation of the wavelet, and that using the WT of $K(\mathbf{x})$ enables one to analyze the spatial distribution of the permeability at increasingly coarser ($a > 1$) or finer ($a < 1$) length scales. As is well-known, $\mathcal{D}(a, \mathbf{b})$ contains information on the *differences* between two approximations of $K(\mathbf{x})$ in two *successive* length scales. But, information about $K(\mathbf{x})$ at a *fixed* length scale is contained in another wavelet coefficient, the *wavelet approximate* or *wavelet scale coefficient*, defined by

$$\mathcal{S}(a, \mathbf{b}) = \int_{-\infty}^{+\infty} \phi_{ab}(\mathbf{x})K(\mathbf{x})d\mathbf{x}\,, \tag{6}$$

where $\phi_{ab}(\mathbf{x})$ is called the *wavelet scaling function* and is orthogonal to $\psi(\mathbf{x})$, with its definition being similar to that of $\psi_{ab}(\mathbf{x})$. An important property of the WTs, which is most useful to upscaling, is that they are *recursive*; that is, they can be applied in succession to any set of properties produced by using the wavelets, to generate another level of averages and another level of details.

Although we simulate and upscale two-dimensional (2D) computational grids in this paper, they can be applied to 3D with equal facility (Pazhoohesh et al., 2006). We utilize a square grid to each square block of which a permeability (or hydraulic conductivity) K is attributed. A one-level discrete WT is then applied to the permeability field. This means that we upscale the computational grid by a factor of 2 by joining the neighboring blocks, except that the upscaling is not uniform. If the center of a block is at $\mathbf{x} = (i_1, i_2)$, we associate with the WT of the permeabilities of that block a set of four wavelet coefficients, three of which are the wavelet detail coefficients, with the fourth one being the wavelet scale coefficient. More precisely, we compute

$$\mathcal{D}_j^{(d)}(i_1, i_2) = \int_{\Omega} K(x, y)\psi_{j,i_1,i_2}^{(d)}(x, y)dxdy\,, \tag{7}$$

and

$$\mathcal{S}_j(i_1, i_2) = \int_{\Omega} K(x, y)\phi_{j,i_1,i_2}(x, y)dxdy\,, \tag{8}$$

where j is the upscaling level such that $j = 1$ represents the initial resolved grid that we begin the computations with, and Ω represents the domain of the problem or the computational grid. $\mathcal{S}_j(i_1, i_2)$ carries information about $K(\mathbf{x})$ associated with a block with its center at $\mathbf{x}$ in the coarser grid, whereas $\mathcal{D}_j^{(d)}(i_1, i_2)$ is a measure of the difference between $K(\mathbf{x})$ in the current upscaled grid and those of the block's neighbors in the previous finer scale grid, with $d = 1, 2,$ and 3 corresponding to the contrasts, respectively, between the blocks in the x, y, and the diagonal directions.

3.2. Upscaling

To implement the upscaling, we introduce two thresholds, $\epsilon_{\mathcal{S}}$ and $\epsilon_{\mathcal{D}}$. The value of $\epsilon_{\mathcal{S}}$ is a measure of the permeability of the grid blocks associated with the wavelet scale coefficient. For a given level of upscaling [a given j in Eq. (7)], we compute the scale coefficients, normalize them with the largest coefficient, and then set $\epsilon_{\mathcal{S}}$ between 0 and 1 (or set it to be a fraction of the largest of such coefficients if we do not normalize them). Likewise, after computing the wavelet detail coefficients and normalizing them, the threshold $\epsilon_{\mathcal{D}}$, which contains information on the contrast between the permeabilities of the neighboring blocks, is set between 0 and 1 (or a fraction of the largest detail coefficient in the computational grid, if the coefficients are not normalized).

The upscaling procedure is as follows (Ebrahimi and Sahimi, 2002; Mehrabi and Sahimi, 1997). The threshold $\epsilon_{\mathcal{S}}$ is compared with the scale coefficient of each block with its center at (i_1, i_2). If (the normalized) $\mathcal{S}_j(i_1, i_2) > \epsilon_{\mathcal{S}}$, it means that the block's permeability K is large and significant. Thus, we do nothing and move on to the next block. If, however, (the normalized) $\mathcal{S}_j(i_1, i_2) < \epsilon_{\mathcal{S}}$, the block's (normalized) detail coefficients $\mathcal{D}_j^{(d)}(i_1, i_2)$ are inspected and set to zero if they are smaller than their threshold $\epsilon_{\mathcal{D}}$. Doing so implies that the neighbor of the block centered at (i_1, i_2) corresponding to the direction (d), which in the finer-scale computational grid is just one horizontal, or vertical, or diagonal block away from (i_1, i_2), is merged with that centered at (i_1, i_2) to form a larger block. Therefore, depending on the broadness and structure of the spatial distribution of $K(\mathbf{x})$ and the numerical values of the two thresholds, a number of blocks in the finer-scale grid are upscaled.

We then take advantage of the recursive property of the WTs, and upscale the new grid further by applying the discrete WT to the scale coefficients obtained at the previous level j (recall that the scale coefficient contain information about the spatial distribution of the permeabilities at a fixed scale), and computing a new set of four wavelet coefficients for each block of the grid in its current state. The newly-computed (normalized) detail coefficients are again set to zero if they are smaller than the threshold $\epsilon_{\mathcal{D}}$, and the corresponding blocks in the grid are merged. The iterative process for upscaling is repeated again until no significant number of the grid blocks is upscaled (merged). Typically, for given values of the two thresholds, three or four levels of coarsening j suffice to generate an upscaled grid that can no longer be upscaled significantly. Therefore, the procedure yields very quickly the final upscaled grid. It should be clear that larger thresholds result in larger number of the grid blocks that are upscaled, and are set by both the required accuracy and the amount of computational time that one can afford.

The next step is computing the effective permeabilities of the upscaled blocks. They may be computed by any of several methods. One way is by *reconstructing* the spatial distribution of the

permeability of the upscaled grid. This means that we compute the inverse WT of $K(\mathbf{x})$ after upscaling the grid (given that many of the detail and scale coefficients are now zero) and assign the permeability of the enlarged upscaled blocks based on the *reconstructed distribution*. What we use in this paper is based on the analogy between the laws of electrical circuits and fluid flow. Thus, for example, an enlarged upscaled block that consists of four neighboring smaller blocks, each having its own permeability, is replaced after upscaling by a larger block with an equivalent permeability K_e given by

$$K_e = \frac{4(K_1+K_3)(K_2+K_4)[K_2K_4(K_1+K_3)+K_1K_3(K_2+K_4)]}{\alpha(\sum_{i=1}^{4}K_i)+3\zeta}\,, \quad (9)$$

with

$$\alpha = K_2K_4(K_1+K_3)+K_1K_3(K_2+K_4)$$
$$\zeta = (K_1+K_2)(K_3+K_4)(K_1+K_3)(K_2+K_4)$$

and K_i $(i=1-4)$ are the permeabilities of the four blocks (Ebrahimi and Sahimi, 2004). The key attribute of this method, in addition to its simplicity, is that no important information about the permeability field is lost, because the permeabilities of the smaller blocks are used in a rigorous manner for computing K_e. If the permeabilities are direction-dependent, as in anisotropic porous media, then Eq. (9) is used once for each direction in order to compute the equivalent direction-dependent permeabilities.

3.3. The wavelets

Because we work with 2D computational grids, we must specify 2D wavelets. One way of constructing 2D wavelets used in the present paper is by tensor products of 1D wavelets, which produces a 2D wavelet scaling function, $\phi_{j,i_1,i_2}(x,y)=\phi^j_{i_1}(x)\phi^j_{i_2}(y)$, and three wavelets:

$$\psi^{(1)}_{j,i_1,i_2}(x,y) = \phi^j_{i_1}(x)\psi^j_{i_2}(y)\,,$$
$$\psi^{(2)}_{j,i_1,i_2}(x,y) = \psi^j_{i_1}(x)\phi^j_{i_2}(y)\,,$$
$$\psi^{(3)}_{j,i_1,i_2}(x,y) = \psi^j_{i_1}(x)\psi^j_{i_2}(y)\,. \quad (10)$$

The 1D discrete wavelets themselves are constructed by setting $a=2^j$ and $b=2^j i$ in Eqs. (5) and (6), where i and j are both integer. By rescaling and translating $\psi(x)$ and $\phi(x)$ using $\psi^j_i(x)=2^{-j/2}\psi(2^{-j}x-i)$, and $\phi^j_i(x)=2^{-j/2}\phi(2^{-j}x-i)$, one also constructs orthonormal wavelets that are non-zero over only small intervals of x. The compact support of the wavelets is important, because it makes the computations extremely rapid.

An important set of wavelets, developed by Daubechies (1988), consists of orthonormal wavelets of order M, and referred to as the DBM. Their first M moments are zero, hence the name. Moreover,

$$\phi(x) = \sqrt{2}\sum_{i=0}^{L-1} h_i\phi(2x-i)\,, \quad (11)$$

$$\psi(x) = \sqrt{2}\sum_{i=0}^{L-1} g_i\phi(2x-i)\,, \quad (12)$$

where $L=2M$, with h_i and g_i - referred to as the *filter coefficients* - are related by, $g_i=(-1)^i h_{L-i-1}$, with $i=0,1,\cdots,L-1$. These coefficients are usually nonzero for only a few values of i. For example, for the DB2 wavelet, one has, $(h_0,h_1,h_2,h_3)=(1/4\sqrt{2})(1+\sqrt{3},3+\sqrt{3},3-\sqrt{3},1-\sqrt{3})$, and $(g_0,g_1,g_2,g_3)=(-h_3,h_2,-h_1,h_0)$. Note that in both cases the extra factor $1/\sqrt{2}$ is necessary to ensure the orthonormality of ϕ and ψ. Press et al. (2007) provide the numerical values of h_k for many wavelets. Based on our previous work for upscaling of flow and transport (Ebrahimi and Sahimi, 2002, 2004, 2006, Heidarinasab et al., 2004; Mehrabi and Sahimi, 1997; Rasaei and Sahimi, 2008, 2009; Sahimi, 2003), the results reported in this paper were computed by using the DB4 wavelet, for which the filter coefficients $(h_0,\ h_1,\ h_2,\ h_3)$ are, $\frac{1}{8}[(\sqrt{2}+\sqrt{6}),(3\sqrt{2}+\sqrt{6}),(3\sqrt{2}-\sqrt{6}),\ (\sqrt{2}-\sqrt{3})]$. We have previously shown that the use of more complex wavelets will not result in much improved results. Note that the scale and translation parameters of the model wavelet, i.e. a and b, are set by the physical constraints that one imposes on the wavelets, which in turn depend on the particular application.

4. The spatial distribution of the permeability and numerical simulation

We consider flow and transport in a spatially-heterogeneous aquifer, and generate several broad distributions of the hydraulic conductivity in an initially uniform computation grid with square blocks of size $\Delta_x=\Delta_y=\Delta$ and various grid sizes $L\times L$ (i.e. size of the computational domain). In all the simulations and for all domain sizes L, we set $\Delta=1$ m. We opt to generate the conductivity fields according to a fractional Brownian motion (fBm), which is a stochastic process that induces long-range correlations in the hydraulic conductivity field. Our choice is not a limitation; any other field with other types of correlation functions may be adopted. It is important to note that the methodology described in this paper is completely general and can be used with any conductivity field, such as multi-Gaussian fields (Kitanidis, 1997; Rubin, 2003), non-Gaussian fields (Zinn and Harvey, 2003) and composite medium (Winter and Tartakovsky, 2002). It can also be used with random fields characterized by Gaussian or exponential covariance models. At the same time, we point out that many field data acquired for oil reservoirs and aquifers display the fBm-type correlations (Benson et al., 2002; Di Federico and Neuman, 1998; Hewett et al., 1986; Molz et al., 2004; Neuman et al., 2008; Riva et al., 2015; Sahimi, 2011; Sahimi and Tajer, 2005), after the original work of Hewett et al. (1986) who demonstated the existence of such long-range correlations in the porosity logs. The two-point correlation function of the fBm is given by

$$\mathcal{C}(\mathbf{r})-\mathcal{C}(\mathbf{0})\sim\mathbf{r}^{2H}\,, \quad (13)$$

where $\mathbf{r}$ is the lag-distance and H is the Hurst exponent. For $0<H<0.5$, the field's hydraulic conductivities are negatively correlated, whereas for $0.5<H<1$ they are positively correlated. Negative correlations imply that a grid block with a high or low conductivity is less likely to be a neighbor to another grid block with a high or low conductivity. The opposite is true for positive correlations. To study the effect of the nature of the correlations - positive versus negative - simulations were carried out for four values of H that are listed in Table 1 and referred to as the "First scenario." Note that a conductivity field with $H<0.5$ represents a much more heterogeneous porous medium than one with $H>0.5$. Furthermore, in order to examine the effect of the broadness of the conductivity distribution on the effectiveness of the upscaling method, three distinct orders of magnitude variations, S in the K values were considered in the numerical experiments, which are also listed in Table 1 and referred to as the "Second scenario." Finally, the performance of the WT upscaling was investigated with various domain sizes listed in Table 1 and referred to as the "Third scenario."

All the conductivity fields were upscaled with the thresholds $\epsilon_{\mathcal{S}}=\epsilon_{\mathcal{D}}=0.9$. Such high thresholds imply that a very large fraction of the blocks are upscaled but, as we demonstrate below, even they produce very accurate results. In the numerical simulations described below the maximum level of upscaling was 3,

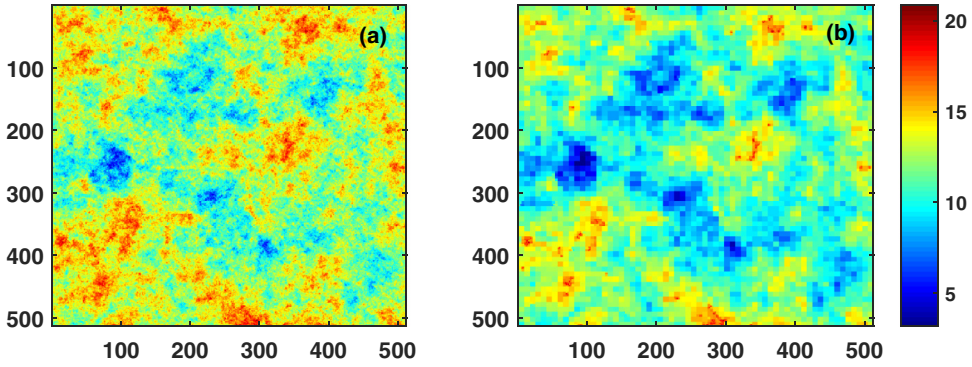

Fig. 1. Comparison of (a) the conductivity field in the high-resolution model of size $L = 512$ m with the Hurst exponent $H = 0.2$ and the order of magnitude variations of the K values, $S = 3$, and (b) the corresponding upscaled field.

Table 1
Summary of the parameters used in the simulations. $\mathcal{R}$ is the measure of the reduction in the number of grid blocks defined by $\mathcal{R} = (n_f - n_c)/n_f \times 100\%$ and x_{CP} is the location of the control plane where the concentration breakthrough curves are evaluated.

Scenarios	L	H	S	$\mathcal{R}(\%)$	x_{CP}
First Scenario	512	0.2	3	97.80	350
	512	0.4	3	98.08	350
	512	0.6	3	98.11	350
	512	0.8	3	98.27	350
Second Scenario	512	0.7	3	98.20	350
	512	0.7	5	96.57	350
	512	0.7	7	98.23	350
Third Scenario	256	0.7	3	97.71	150
	512	0.7	3	98.40	350
	1024	0.7	3	97.45	500

since higher levels of upscaling did not result in much coarser computational grids. As an example, Fig. 1 presents a fine-scale conductivity field used in the study with $L = 512$ m, $H = 0.2$ and $S = 3$, together with the corresponding upscaled model. Let n_c and n_f denote, respectively, the number of grid blocks in the coarsened field and in the initial fine-grid structure. We define $\mathcal{R} = (n_f - n_c)/n_f \times 100\%$ as the measure of the reduction in the number of grid blocks that we achieve by the WT upscaling. This quantity is also listed in Table 1.

Flow is simulated by solving Eq. (2) in both the fine and coarse permeability fields. No-flow boundary conditions along the transverse boundaries are used, and a constant longitudinal head gradient is imposed between the leftmost and rightmost sides of the grid with their values being, respectively, 2 m and 1 m. As for the transport simulation, we solve for the case in which we inject a non-reactive tracer along a transverse line source. The tracer is released with constant flow rate, $q = 40$ m^2/d, at the left side of the computational grid.

We evaluate the breakthrough concentration of the plume at a control plane (CP) with a longitudinal location x_{CP} from the line source. For each scenario, the value of x_{CP} is listed in Table 1. Solute transport is simulated by solving Eq. (3 or 4) by a random walk method, with its detailed description reported in Araktingi et al. (1993); Ebrahimi and Sahimi (2004); King and Scher (1987). The longitudinal and transverse dispersion at the local-scale were 0.546 m^2/d and 0.0045 m^2/d, respectively. For each case, several realizations of the conductivity fields were generated and the results were averaged over all of them.

5. Results and discussion

Fig. 2 compares the plume's snapshots in both the high-resolution and upscaled computational grids for two distinct times. The temporal evolution of the concentration is expressed in terms of pore volume injected (PVI). The PVI is the fractional volume of the fluid injected relative to the total pore volume of the pore space. With uniform injection, as we do in this work, the PVI is the dimensionless time. The size of the grid is $L = 512$ m with the Hurst exponent being $H = 0.2$. The order of magnitude variations in the hydraulic conductivity is $S = 3$. As Fig. 2 indicates, the concentration profiles in the upscaled field reproduce very accurately the results obtained with the corresponding fine-scale geological model.

We also analyzed systematically the influence of three important parameters of the upscaling, namely, the Hurst exponent H, the order of magnitude variations in the conductivities, S, and the size L of the computational grid. The travel time of plumes is controlled by the correlations and contrast between the conductivities of the different zones of a porous medium. Thus, we highlight the effects of H and S, as the Hurst exponent characterizes the nature of the correlations between the conductivities, while S quantifies the broadness of their spatial distribution.

Fig. 3 compares quantitatively the concentration profiles at the CP in the highly resolved and coarsened computational grids for four values of H. There is very little, if any, difference between the profiles, demonstrating the accuracy of the upscaling algorithm. Furthermore, in order to demonstrate the agreement between the results obtained from the fine-scale and upscaled fields, goodness-of-fit analysis was carried out and depicted in Fig. 4 for the case with $L = 512$ m, $H = 0.8$ and $S = 3$. The equation of the straight line fitted to the contaminant concentration data in Fig. 4 is $y = 0.99x + 1.7$ with $R^2 = 0.9997$, where y and x are associated with the upscaled and fine-scale data, respectively. As Fig. 3 demonstrates, for the K fields with $H > 0.5$, in which the conductivities are positively correlated and better connected flow and transport paths exist, the breakthrough occurs earlier than that in the K fields with $H < 0.5$. Note also the ability of the algorithm for capturing the precise first arrival times (in the PVIs), which are critical for risk analysis (Henri et al., 2015).

Fig. 5 presents the dependence of $\mathcal{R}$, the percentage of the remaining grid blocks in the final upscaled computational grid, on the Hurst exponent H. $\mathcal{R}$ is slightly larger for $H < 0.5$, since the conductivity fields with negative long-range correlations represent more heterogeneous porous media. But, overall, for all $0 < H < 1$ the upscaled grid is extremely coarsened, having a very small number of enlarged grid blocks and yet, as Figs. 2 and 3 indicate, the accuracy of the concentration profiles in such grids is

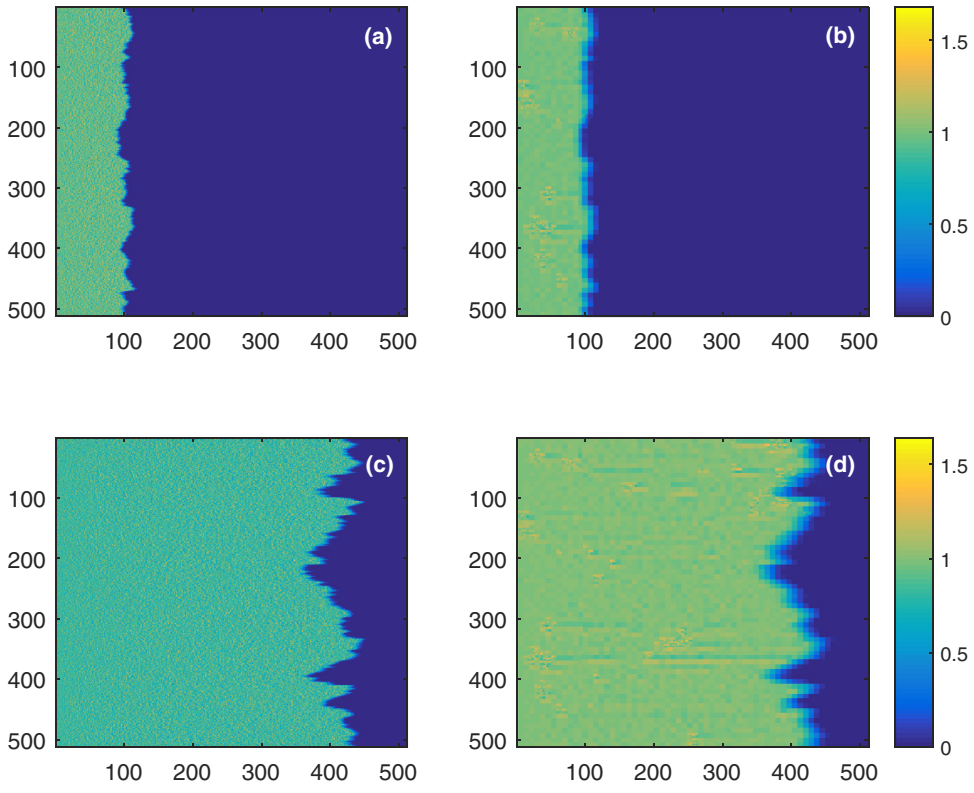

Fig. 2. Solute plume snapshots for the high-resolution and coarse-scale conductivity fields. The concentration $C(\mathbf{x}, t)$ was computed in both high-resolution and coarse-scale conductivity fields for the parameters, $L = 512$ m, $H = 0.2$ and $S = 3$, and for (a) high-resolution field at PVI $= 0.2$; (b) coarsened field at PVI $= 0.2$; (c) high-resolution field at PVI $= 0.8$, and (d) coarsened field at PVI $= 0.8$.

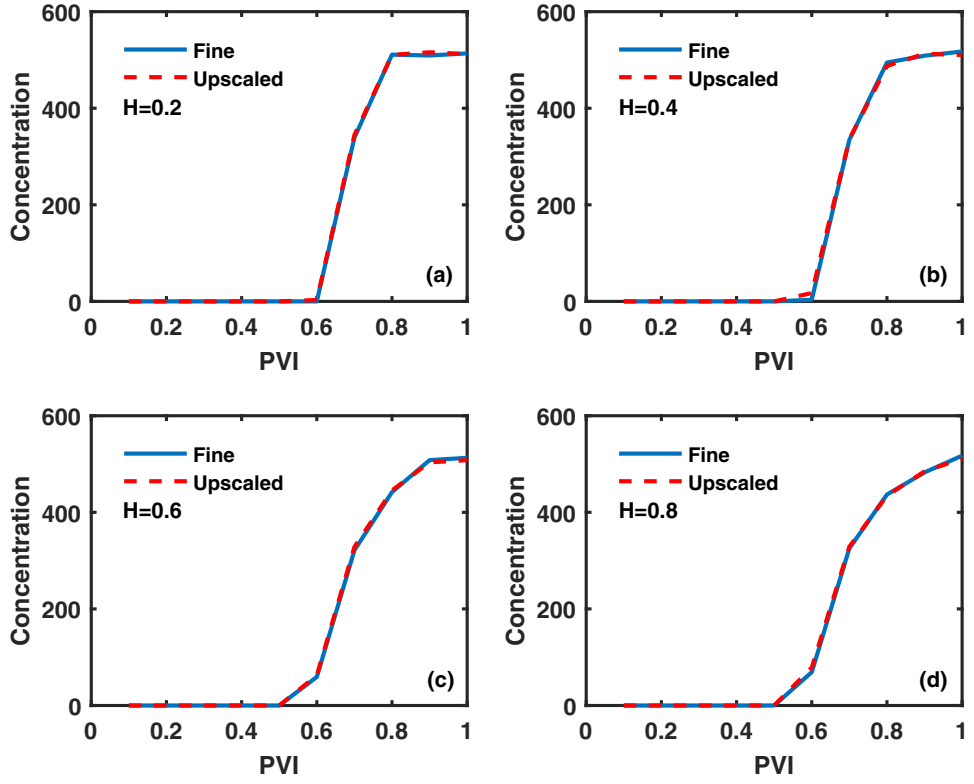

Fig. 3. The results for the first scenario (see Table 1): Concentration breakthrough curves for the high-resolution fields with $S = 3$ and dimension $L = 512$ m and the corresponding coarsened fields. Results shown for (a) $H = 0.2$; (b) $H = 0.4$; (c) $H = 0.6$, and (d) $H = 0.8$.

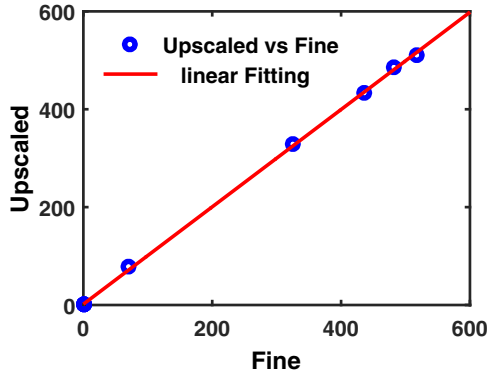

Fig. 4. Goodness-of-fit analysis between the concentration profiles obtained from fine-scale and upscaled fields for the case with $L = 512$ m, $H = 0.8$ and $S = 3$. The straight line is represented by $y = 0.99x + 1.7$ with $R^2 = 0.9997$.

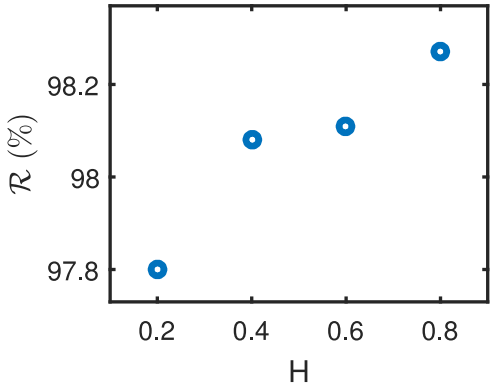

Fig. 5. The percent reduction, $\mathcal{R}$, of the number of grid blocks in the upscaled fields and that of the grid representing the corresponding high-resolution fields, and its dependence on the Hurst coefficient H in the first scenario (see Table 1).

completely comparable with that of the fine-scale grids. As pointed out by Ebrahimi and Sahimi (2002, 2004, 2006), the wavelet scale coefficients preserve the distribution of the high permeability paths, while the wavelet detail coefficients preserve the grid resolution where the permeability contrasts are high, such as the interface between the low and high permeabilities. These are, of course, precisely what are expected of any accurate upscaling scheme. Thus, the WT upscaling is completely suitable for geological domains displaying fast flow paths induced by the persistence of high conductivities, but also for more heterogeneous porous formations in which slow transport paths may develop.

Next, we examine the sensitivity of the upscaling scheme to S, the order of magnitude variations in the hydraulic conductivity field, referred to as the second scenario in Table 1. Fig. 6 compares the concentration profiles for $S = 3$, 5 and 7. Even when there are seven orders of magnitude variations in the values of K, the breakthrough points (BTPs) are predicted accurately by the upscaled scheme, and the concentration profiles in all three cases in the coarsened and fine-resolution grids agree excellently. There is only a slight discrepancy between the fine- and coarse-scale fields for $S = 7$ around PVI $= 0.7$, but all other main features of the profiles are captured (including the first arrival times) even for $S = 7$. In their study of frequency-dependence conductivity in highly heterogeneous semiconducting materials in which the local conductivities vary up to 15 orders of magnitude, Pazhoohesh et al. (2006) demonstrated that, in fact, broader conductivity distributions lead to more accurate results and more efficient computations, because only a very small fraction of highly

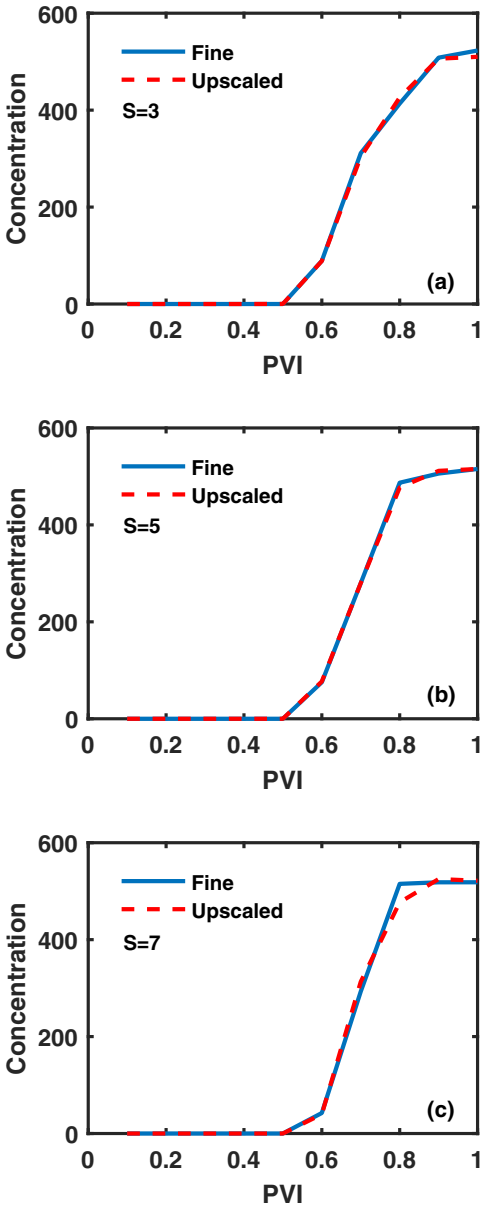

Fig. 6. Results obtained for the second scenario (see Table 1). Comparison between the concentration breakthrough curves for coarsened and fine scale conductivity fields for $H = 0.7$ and grid size $L = 512$ m. Results reported for (a) $S = 3$; (b) $S = 5$, and (c) $S = 7$.

heterogeneous media contribute significantly to transport, and the WT upscaling identifies them accurately.

We present in Fig. 7 the effect of the domain's size L on the upscaling procedure. It presents comparisons of the concentration profiles in three computational grids with increasing sizes. Increasing the size of grid results in more accurate, and hence computationally more efficient results. For $L = 1024$ m, the two profiles are virtually identical.

Since the dispersion coefficients essentially represent the second spatial moments of the concentration distribution, we also computed S_{xx}, the second central moment of the plume in the longitudinal direction that represents the spread of the solute body around its centroid. The second central spatial moment S_{xx} is given by

$$S_{xx}(t) = \mu_{xx}(t) - [\mu_x(t)]^2 \,, \tag{14}$$

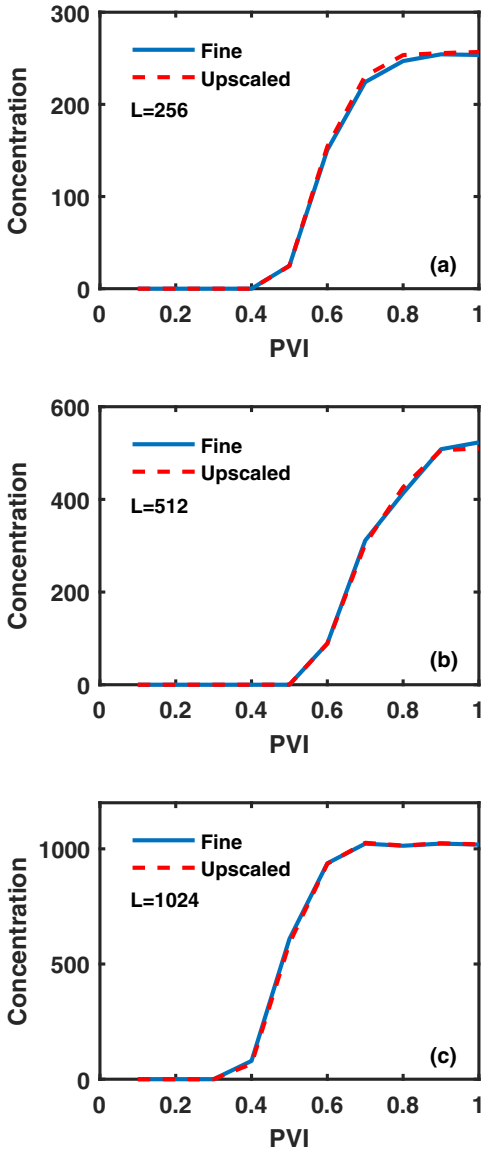

Fig. 7. Results for the third scenario (see Table 1): The breakthrough curves for the high-resolution conductivity fields with $H = 0.7$ and $S = 3$ and the corresponding coarsened fields with (a) $L = 256$ m; (b) $L = 512$ m and (c) $L = 1024$ m.

where

$$\mu_{xx}(t) = \frac{1}{\mu_0(t)}\mathcal{P}\int\int_{\Omega} x^2 C(x,y,t)dxdy\ , \tag{15}$$

$$\mu_{x}(t) = \frac{1}{\mu_0(t)}\mathcal{P}\int\int_{\Omega} xC(x,y,t)dxdy\ , \tag{16}$$

with $\mu_0(t) = \mathcal{P}\int\int_{\Omega} C(x,y,t)dxdy$, which equals to the mass in the domain, and the rest of the notation is as before. In Fig. 8 we present the results for two cases. Fig. 8(a) depicts the results for the case, $H = 0.2$ and $S = 3$, while Fig. 8(b) shows those for $H = 0.7$ and $S = 7$. The linear size of the grid for both cases was $L = 512$. It is clear that there is very little, if any difference between the computed second moments in the high-resolution and upscaled grids, implying that the longitudinal dispersion coefficient is provided highly accurately by the upscaling method.

Note that in all the cases discussed, flow and transport were simulated in the absence of sinks and sources. As demonstrated by Rasaei and Sahimi (2008, 2009), who studied upscaling of two-phase flow in oil reservoirs, in the presence of sinks and sources, such as injection and production wells in such reservoirs, the grid resolution strategy should be adaptive since, due to the high velocity gradients in their vicinity, more refined grid blocks are required around them. Likewise, fully-refined grid blocks are required close to the boundaries where we need to capture the details of the flow and transport processes. To implement this, a simple constraint is imposed on the upscaling process that prevents marked areas around sources, sinks and boundaries from being coarsened.

The results reveal that the wavelet-based upscaling method is accurate for a single disordered porous medium. This is not, however, a limitation as the method can be extended to stochastic hydrogeology. Using a Monte Carlo framework one can, after generating multiple realizations of the heterogeneous fields, upscale the conductivity fields. Then, simulation of flow and transport processes can be carried out through the upscaled conductivity fields.

6. Efficiency of the calculation

One purpose of the present work was to demonstrate that if one upscales a heterogeneous conductivity field by the WT method, simulation of solute transport in the upscaled field yields results for the characteistics of the transport phenomenon that are as accurate as those obtained with the original high-resolution grid. *This is independent of the numerical method that one uses to solve the ADE.* Clearly, if one uses an efficient and accurate numerical scheme for solving the ADE, then the speed-up in the computations will be very large. In the present work, we used a simple random walk method to solve the ADE, which is not necessarily the most efficient method, but has the advantage that it avoids to a large extent numerical dispersion associated with other methods that are used to solve the ADE. The previous work on upscaling of flow of two-immiscible fluids in large-scale porous media (Rasaei and Sahimi, 2008, 2009), which used a finite-volume method, demonstrated that the speed-up in the computations is as large as a factor of 5,000. We expect the same order of speed-up if a similar numerical scheme is used. It was also demonstrated in previous works (Rasaei and Sahimi, 2008, 2009), how to eliminate possible numerical dispersion.

7. Summary

This work presents the application of a methodology for upscaling of the spatial distribution of a hydraulic conductivity or permeability field in a computational grid for simulation of solute transport in spatially-heterogeneous geological formations. The methodology is based on the wavelet transforms that preserve the resolution of the high-conductivity paths, as well as that of the regions in which there are sharp contrasts between the conductivities. The performance of the method was tested for a wide range of the important parameters of the simulations, ranging from the order of magnitude variations in the conductivities and the nature of their correlations (positive versus negative), to the size of the computational grid. We demonstrated in all cases that the upscaled grid constructed by the wavelet transform reproduces the concentration breakthrough curves very accurately when compared with the same in the initial highly-resolved grids. In particular, the breakthrough times are predicted extremely accurately. From a computational point of view, the wavelet transform upscaling method generates non-uniform grids with a number of grid blocks that represent, on average, only about 2.1% of the number of grid blocks in the original high-resolution models. Thus, given any reasonable method of solving the advection-dispersion equation, the upscaling method results in an enormous reduction in the computational time of such simulations.

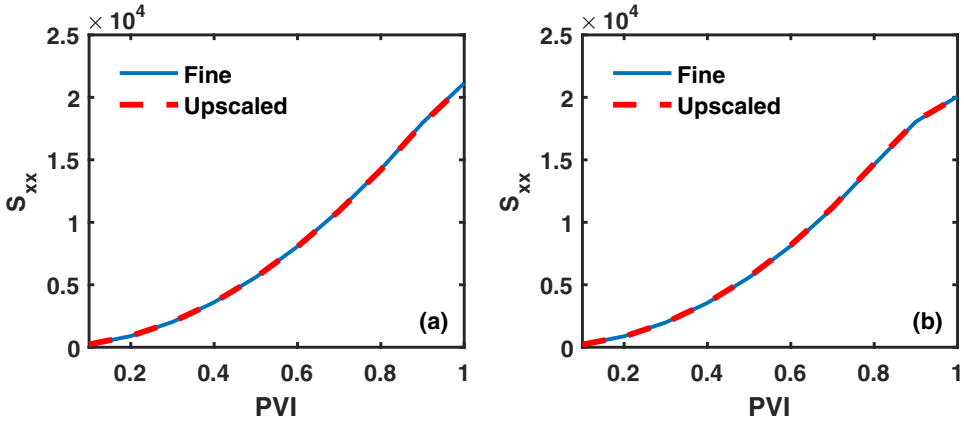

Fig. 8. Comparison of the second central spatial moment $S_{xx}(t)$ of the concentration distribution in the high-resolution and upscaled conductivity fields. The results are for (a) $H = 0.2$ and $S = 3$, and (b) $H = 0.7$ and $S = 7$ (see Table 1). The size of the numerical grid is $L = 512$ and the porosity is equal to 0.54.

References

Ababou, R., 1988. Three-Dimensional Flow in Random Porous Media. Ph.D. thesis Massachusetts Institute of Technology.

Ababou, R., McLaughlin, D., Gelhar, L., Tompson, A., 1989. Numerical simulation of three-dimensional saturated flow in randomly heterogeneous porous media. Transport Porous Med. 4 (6), 549–565. http://dx.doi.org/10.1007/BF00223627.

Araktingi, U.G., Orr Jr, F., et al., 1993. Viscous Fingering in Heterogeneous Porous Media. SPE Adv. Technol. Ser. 1 (01), 71–80. http://dx.doi.org/10.2118/18095-PA.

Attinger, S., 2003. Generalized coarse graining procedures for flow in porous media. Computat. Geosci. 7 (4), 253–273. http://dx.doi.org/10.1023/B:COMG.0000005243.73381.e3.

de Barros, F.P.J., Dentz, M., 2016. Pictures of blockscale transport: effective versus ensemble dispersion and its uncertainty. Adv. Water Resour. 91, 11–22. http://dx.doi.org/10.1016/j.advwatres.2016.03.004.

de Barros, F.P.J., Fiori, A., 2014. First-order based cumulative distribution function for solute concentration in heterogeneous aquifers: theoretical analysis and implications for human health risk assessment. Water Resour. Res. 50 (5), 4018–4037. http://dx.doi.org/10.1002/2013WR015024.

de Barros, F.P.J., Rubin, Y., 2008. A risk-driven approach for subsurface site characterization. Water Resour. Res. 44 (1), W01414. http://dx.doi.org/10.1029/2007WR006081.

de Barros, F.P.J., Rubin, Y., 2011. Modelling of block-scale macrodispersion as a random function. J. Fluid Mech. 676, 514–545. http://dx.doi.org/10.1017/jfm.2011.65.

Benson, D.A., Schumer, R., Meerschaert, M.M., Wheatcraft, S.W., 2002. Fractional dispersion, lévy motion, and the made tracer tests. In: Dispersion in Heterogeneous Geological Formations. Springer, pp. 211–240. http://dx.doi.org/10.1007/978-94-017-1278-1_11.

Chui, C.K., 1992. Wavelet Analysis and Its Applications. Academic press.

Dagan, G., 1984. Solute transport in heterogeneous porous formations. J. Fluid Mech. 145, 151–177. http://dx.doi.org/10.1017/S0022112084002858.

Dagan, G., et al., 1989. Flow and Transport in Porous Formations.. Springer-Verlag GmbH & Co. KG..

Daubechies, I., 1988. Orthonormal bases of compactly supported wavelets. Commun. Pur. App. Math. 41 (7), 909–996. http://dx.doi.org/10.1002/cpa.3160410705.

Dentz, M., Le Borgne, T., Englert, A., Bijeljic, B., 2011. Mixing, spreading and reaction in heterogeneous media: a brief review. J. Contam. Hydrol. 120, 1–17. http://dx.doi.org/10.1016/j.jconhyd.2010.05.002.

Dentz, M., Tartakovsky, D.M., 2010. Probability density functions for passive scalars dispersed in random velocity fields. Geophys Res. Lett. 37 (24), L24406. http://dx.doi.org/10.1029/2010GL045748.

Desbarats, A., 1992. Spatial averaging of hydraulic conductivity in three-dimensional heterogeneous porous media. Math. Geol. 24 (3), 249–267. http://dx.doi.org/10.1007/BF00893749.

Desbarats, A.J., 1987. Numerical estimation of effective permeability in sand-shale formations. Water Resour. Res. 23 (2), 273–286. http://dx.doi.org/10.1029/WR023i002p00273.

Di Federico, V., Neuman, S.P., 1998. Transport in multiscale log conductivity fields with truncated power variograms. Water Resour. Res. 34 (5), 963–973. http://dx.doi.org/10.1029/98WR00221.

de Dreuzy, J.-R., Beaudoin, A., Erhel, J., 2007. Asymptotic dispersion in 2d heterogeneous porous media determined by parallel numerical simulations. Water Resour. Res. 43 (10), W10439. http://dx.doi.org/10.1029/2006WR005394.

Durlofsky, L.J., 1991. Numerical calculation of equivalent grid block permeability tensors for heterogeneous porous media. Water Resour. Res. 27 (5), 699–708. http://dx.doi.org/10.1029/91WR00107.

Durlofsky, L.J., Jones, R.C., Milliken, W.J., 1997. A nonuniform coarsening approach for the scale-up of displacement processes in heterogeneous porous media. Adv. Water Resour. 20 (5), 335–347. http://dx.doi.org/10.1016/S0309-1708(96)00053-X.

Ebrahimi, F., Sahimi, M., 2002. Multiresolution wavelet coarsening and analysis of transport in heterogeneous media. Physica A 316 (1), 160–188. http://dx.doi.org/10.1016/S0378-4371(02)01199-8.

Ebrahimi, F., Sahimi, M., 2004. Multiresolution wavelet scale up of unstable miscible displacements in flow through heterogeneous porous media. Transport Porous Med. 57 (1), 75–102. http://dx.doi.org/10.1023/B:TIPM.0000032742.05517.06.

Ebrahimi, F., Sahimi, M., 2006. Grid coarsening, simulation of transport processes in, and scale-up of heterogeneous media: application of multiresolution wavelet transformations. Mech. Mater. 38 (8), 772–785. http://dx.doi.org/10.1016/j.mechmat.2005.06.013.

Fiori, A., Dagan, G., Jankovic, I., 2011. Upscaling of steady flow in three-dimensional highly heterogeneous formations. Multiscale Model. Simul. 9 (3), 1162–1180. http://dx.doi.org/10.1137/110820294.

Gelhar, L.W., Axness, C.L., 1983. Three-dimensional stochastic analysis of macrodispersion in aquifers. Water Resour. Res. 19 (1), 161–180. http://dx.doi.org/10.1029/WR019i001p00161.

Gutjahr, A.L., Gelhar, L.W., Bakr, A.A., MacMillan, J.R., 1978. Stochastic analysis of spatial variability in subsurface flows: 2. evaluation and application. Water Resour. Res. 14 (5), 953–959. http://dx.doi.org/10.1029/WR014i005p00953.

Heidarinasab, A., Dabir, B., Sahimi, M., 2004. Multiresolution wavelet-based simulation of transport and photochemical reactions in the atmosphere. Atmos. Environ. 38 (37), 6381–6397. http://dx.doi.org/10.1016/j.atmosenv.2004.08.024.

Henri, C.V., Fernàndez-Garcia, D., de Barros, F.P.J., 2015. Probabilistic human health risk assessment of degradation-related chemical mixtures in heterogeneous aquifers: risk statistics, hot spots, and preferential channels. Water Resour. Res. 51 (6), 4086–4108. http://dx.doi.org/10.1002/2014WR016717.

Hewett, T., et al., 1986. Fractal distributions of reservoir heterogeneity and their influence on fluid transport. In: SPE Annual Technical Conference and Exhibition. Society of Petroleum Engineers http://dx.doi.org/10.2118/15386-MS.

Holschneider, M., 1995. Wavelets, An Analysis Tool. Oxford University Press.

Kikani, J., He, M., et al., 1998. Multi-resolution analysis of long-term pressure transient data using wavelet methods. In: SPE Annual Technical Conference and Exhibition. Society of Petroleum Engineers http://dx.doi.org/10.2118/48966-MS.

King, M.J., Scher, H., 1987. Probability approach to multiphase and multicomponent fluid flow in porous media. Phys. Rev. A 35 (2), 929. http://dx.doi.org/10.1103/PhysRevA.35.929.

King, P., 1989. The use of renormalization for calculating effective permeability. Transport Porous Med. 4 (1), 37–58. http://dx.doi.org/10.1007/BF00134741.

King, P., Muggeridge, A., Price, W., 1993. Renormalization calculations of immiscible flow. Transport Porous Med. 12 (3), 237–260. http://dx.doi.org/10.1007/BF00624460.

Kitanidis, P., 1997. Introduction to Geostatistics: Applications in Hydrogeology. Cambridge University Press.

Kitanidis, P.K., 1990. Effective hydraulic conductivity for gradually varying flow. Water Resour. Res. 26 (6), 1197–1208. http://dx.doi.org/10.1029/WR026i006p01197.

Koch, D.L., Brady, J.F., 1985. Dispersion in fixed beds. J. Fluid Mech. 154, 399–427. http://dx.doi.org/10.1017/S0022112085001598.

Leube, P.C., de Barros, F.P.J., Nowak, W., Rajagopal, R., 2013. Towards optimal allocation of computer resources: trade-offs between uncertainty quantification, discretization and model reduction. Environ. Model. Softw. 50, 97–107. http://dx.doi.org/10.1016/j.envsoft.2013.08.008.

Leube, P.C., Nowak, W., Schneider, G., 2012. Temporal moments revisited: why there is no better way for physically based model reduction in time. Water Resour. Res. 48 (11), W11527. http://dx.doi.org/10.1029/2012WR011973.

Lu, P., Horne, R.N., et al., 2000. A multiresolution approach to reservoir parameter estimation using wavelet analysis. In: SPE Annual Technical Conference and Exhibition. Society of Petroleum Engineers http://dx.doi.org/10.2118/62985-MS.

Luo, J., Dentz, M., Carrera, J., Kitanidis, P., 2008. Effective reaction parameters for mixing controlled reactions in heterogeneous media. Water Resour. Res. 44 (2), W02416. http://dx.doi.org/10.1029/2006WR005658.

Maxwell, R.M., Kastenberg, W.E., Rubin, Y., 1999. A methodology to integrate site characterization information into groundwater-driven health risk assessment. Water Resour. Res. 35 (9), 2841–2855. http://dx.doi.org/10.1029/1999WR900103.
Mehrabi, A.R., Sahimi, M., 1997. Coarsening of heterogeneous media: application of wavelets. Phys. Rev. Lett. 79 (22), 4385–4388. http://dx.doi.org/10.1103/PhysRevLett.79.4385.
Meyer, Y., 1992. Wavelets and Applications. Springer.
Molz, F.J., Rajaram, H., Lu, S., 2004. Stochastic fractal-based models of heterogeneity in subsurface hydrology: origins, applications, limitations, and future research questions. Rev. Geophys. 42 (1), RG1002. http://dx.doi.org/10.1029/2003RG000126.
Moridis, G., Nikolaou, M., You, Y., et al., 1996. The use of wavelet transforms in the solution of two-phase flow problems. Soc. Petrol Eng. J. 1 (02), 169–178. http://dx.doi.org/10.2118/29144-PA.
Moslehi, M., Rajagopal, R., de Barros, F.P.J., 2015. Optimal allocation of computational resources in hydrogeological models under uncertainty. Adv. Water Resour. 83, 299–309. http://dx.doi.org/10.1016/j.advwatres.2015.06.014.
Mukhopadhyay, S., Sahimi, M., 2000. Calculation of the effective permeabilities of field-scale porous media. Chem. Eng. Sci. 55 (20), 4495–4513. http://dx.doi.org/10.1016/S0009-2509(00)00098-1.
Neuman, S.P., Riva, M., Guadagnini, A., 2008. On the geostatistical characterization of hierarchical media. Water Resour. Res. 44 (2). http://dx.doi.org/10.1029/2007WR006228.
Neuman, S.P., Winter, C.L., Newman, C.M., 1987. Stochastic theory of field-scale fickian dispersion in anisotropic porous media. Water Resour. Res. 23 (3), 453–466. http://dx.doi.org/10.1029/WR023i003p00453.
Nievergelt, Y., 1999. Wavelets Made Easy, 174. Springer.
Pazhoohesh, E., Hamzehpour, H., Sahimi, M., 2006. Numerical simulation of ac conduction in three-dimensional heterogeneous materials. Phys. Rev. B 73 (17), 174206. http://dx.doi.org/10.1103/PhysRevB.73.174206.
Press, W., Teukolsky, S., Vetterling, W., Flannery, B., Numerical recipes 3rd edition: The art of scientific computing, 2007, Cambridge University Press.
Rasaei, M.R., Sahimi, M., 2008. Upscaling and simulation of waterflooding in heterogeneous reservoirs using wavelet transformations: application to the SPE-10 model. Transport Porous Med. 72 (3), 311–338. http://dx.doi.org/10.1007/s11242-007-9152-1.
Rasaei, M.R., Sahimi, M., 2009. Upscaling of the permeability by multiscale wavelet transformations and simulation of multiphase flows in heterogeneous porous media. Comput. Geosci. 13 (2), 187–214. http://dx.doi.org/10.1007/s10596-008-9111-0.
Renard, P., De Marsily, G., 1997. Calculating equivalent permeability: a review. Adv. Water Resour. 20 (5), 253–278. http://dx.doi.org/10.1016/S0309-1708(96)00050-4.
Risken, H., 1984. Fokker-Planck Equation. Springer Berlin Heidelberg, Berlin, Heidelberg.
Riva, M., Panzeri, M., Guadagnini, A., Neuman, S.P., 2015. Simulation and analysis of scalable non-gaussian statistically anisotropic random functions. J. Hydrol. 531, 88–95. http://dx.doi.org/10.1016/j.jhydrol.2015.06.066.
Rubin, Y., 2003. Applied Stochastic Hydrogeology. Oxford University Press, USA.
Rubin, Y., Gómez-Hernández, J.J., 1990. A stochastic approach to the problem of upscaling of conductivity in disordered media: Theory and unconditional numerical simulations. Water Resour. Res. 26 (4), 691–701. http://dx.doi.org/10.1029/WR026i004p00691.
Rubin, Y., Sun, A., Maxwell, R., Bellin, A., 1999. The concept of block-effective macrodispersivity and a unified approach for grid-scale-and plume-scale-dependent transport. J. Fluid Mech. 395, 161–180. http://dx.doi.org/10.1017/S0022112099005868.
Rubinstein, J., Torquato, S., 1989. Flow in random porous media: mathematical formulation, variational principles, and rigorous bounds. J. Fluid Mech. 206, 25–46. http://dx.doi.org/10.1017/S0022112089002211.
Sahimi, M., 2003. Large-scale porous media and wavelet transformations. Comput. Sci. Eng. 5 (4), 75–87. http://dx.doi.org/10.1109/MCISE.2003.1208648.
Sahimi, M., 2011. Flow and transport in porous media and fractured rock: from classical methods to modern approaches. John Wiley & Sons.
Sahimi, M., Hashemi, M., 2001. Wavelet identification of the spatial distribution of fractures. Geophys. Res. lett. 28 (4), 611–614. http://dx.doi.org/10.1029/2000GL011961.
Sahimi, M., Tajer, S.E., 2005. Self-affine fractal distributions of the bulk density, elastic moduli, and seismic wave velocities of rock. Phys. Rev. E 71 (4), 046301. http://dx.doi.org/10.1103/PhysRevE.71.046301.
Wang, J., Kitanidis, P.K., 1999. Analysis of macrodispersion through volume averaging: comparison with stochastic theory. Stoch. Environ. Res. Risk A 13 (1–2), 66–84. http://dx.doi.org/10.1007/s004770050032.
Warren, J., Price, H., et al., 1961. Flow in heterogeneous porous media. Soc. Petrol. Eng. J. 1 (03), 153–169. http://dx.doi.org/10.2118/1579-G.
Wen, X.-H., Gómez-Hernández, J.J., 1996. Upscaling hydraulic conductivities in heterogeneous media: an overview. J. Hydrol. 183 (1), ix–xxxii. http://dx.doi.org/10.1016/S0022-1694(96)80030-8.
Whitaker, S., 1999. The Method of Volume Averaging. Theory and Applications of Transport in Porous Media. Kluwer Academic, The Netherlands.
Winter, C.L., Tartakovsky, D.M., 2002. Groundwater flow in heterogeneous composite aquifers. Water Resour. Res. 38 (8). http://dx.doi.org/10.1029/2001WR000450.
Wood, B.D., Cherblanc, F., Quintard, M., Whitaker, S., 2003. Volume averaging for determining the effective dispersion tensor: closure using periodic unit cells and comparison with ensemble averaging. Water Resour. Res. 39 (8), 1210. http://dx.doi.org/10.1029/2002WR001723.
Wood, B.D., Valdés-Parada, F.J., 2013. Volume averaging: local and nonlocal closures using a green's function approach. Adv. Water Resour. 51, 139–167. http://dx.doi.org/10.1016/j.advwatres.2012.06.008.
Zinn, B., Harvey, C.F., 2003. When good statistical models of aquifer heterogeneity go bad: a comparison of flow, dispersion, and mass transfer in connected and multivariate gaussian hydraulic conductivity fields. Water Resour. Res. 39 (3). http://dx.doi.org/10.1029/2001WR001146.